Atomic-scale electronic structure of the cuprate pair density wave state coexisting with superconductivity

Peayush Choubey[a,b,1], Sang Hyun Joo[c,1], K. Fujita[d], Zengyi Du[d], S. D. Edkins[e], M. H. Hamidian[f], H. Eisaki[g], S. Uchida[g], A. P. Mackenzie[h], Jinho Lee[c], J. C. Séamus Davis[i,j,k,2], and P. J. Hirschfeld[l]

[a]Institut für Theoretische Physik III, Ruhr-Universität Bochum, D-44801 Bochum, Germany; [b]Department of Physics, Indian Institute of Science, 560012 Bengaluru, India; [c]Department of Physics and Astronomy, Seoul National University, 08826 Seoul, Korea; [d]Condensed Matter Physics and Materials Science (CMPMS) Department, Brookhaven National Laboratory, Upton, NY 11973; [e]Department of Applied Physics, Stanford University, Stanford, CA 94305; [f]Department of Physics, Harvard University, Cambridge, MA 02138; [g]Institute of Advanced Industrial Science and Technology, Tsukuba, Ibaraki 305-8568, Japan; [h]Max-Planck Institute for Chemical Physics of Solids, D-01187 Dresden, Germany; [i]Laboratory of Atomic and Solid State Physics (LASSP), Department of Physics, Cornell University, Ithaca, NY 14850; [j]Clarendon Laboratory, University of Oxford, OX1 3PU Oxford, United Kingdom; [k]Department of Physics, University College Cork, T12 R5C Cork, Ireland; and [l]Department of Physics, University of Florida, Gainesville, FL 32611

Contributed by J. C. Séamus Davis, April 22, 2020 (sent for review February 20, 2020; reviewed by Erez Berg and Hermann Suderow)

The defining characteristic of hole-doped cuprates is *d*-wave high temperature superconductivity. However, intense theoretical interest is now focused on whether a pair density wave state (PDW) could coexist with cuprate superconductivity [D. F. Agterberg et al., *Annu. Rev. Condens. Matter Phys.* 11, 231 (2020)]. Here, we use a strong-coupling mean-field theory of cuprates, to model the atomic-scale electronic structure of an eight-unit-cell periodic, *d*-symmetry form factor, pair density wave (PDW) state coexisting with *d*-wave superconductivity (DSC). From this PDW + DSC model, the atomically resolved density of Bogoliubov quasiparticle states $N(\boldsymbol{r}, E)$ is predicted at the terminal BiO surface of $Bi_2Sr_2CaCu_2O_8$ and compared with high-precision electronic visualization experiments using spectroscopic imaging scanning tunneling microscopy (STM). The PDW + DSC model predictions include the intraunit-cell structure and periodic modulations of $N(\boldsymbol{r}, E)$, the modulations of the coherence peak energy $\Delta_p(\boldsymbol{r})$, and the characteristics of Bogoliubov quasiparticle interference in scattering-wavevector space $(\boldsymbol{q}-\text{space})$. Consistency between all these predictions and the corresponding experiments indicates that lightly hole-doped $Bi_2Sr_2CaCu_2O_8$ does contain a PDW + DSC state. Moreover, in the model the PDW + DSC state becomes unstable to a pure DSC state at a critical hole density p^*, with empirically equivalent phenomena occurring in the experiments. All these results are consistent with a picture in which the cuprate translational symmetry-breaking state is a PDW, the observed charge modulations are its consequence, the antinodal pseudogap is that of the PDW state, and the cuprate critical point at $p^* \approx 19\%$ occurs due to disappearance of this PDW.

cuprate pseudogap | pair density wave state | quasiparticle interference

In the elementary undoped CuO_2 plane, each Cu $d_{x^2-y^2}$ orbital is occupied by a single electron and, because the energy required to doubly occupy this orbital is $U \sim 3$ eV, a Mott insulator (MI) state develops (1, 2). The superexchange spin–spin interaction energy between neighboring $d_{x^2-y^2}$ electrons is $J \sim 150$ meV, leading to a robust antiferromagnetic (AF) phase (3, 4) (Fig. 1*A*). However, this AF insulating state vanishes with the removal of as little as 3% of the electrons per Cu site (hole density $p = 3\%$), to reveal the pseudogap (PG) state in a region of the phase diagram bounded by $p < p^*$ and temperatures $T < T^*(p)$ (Fig. 1*A*). Key characteristics of the PG state include (3, 4) a steep drop in both magnetic susceptibility and *c*-axis conductivity; an apparently incomplete Fermi surface consisting of coherent quasiparticle states on four $\boldsymbol{k}$-space arcs neighboring $\boldsymbol{k} \approx (\pm\pi/2a, \pm\pi/2a)$; an energy gap Δ^* in the spectrum of quasiparticle states near $\boldsymbol{k} \approx (\pm\pi/a, 0); (0, \pm\pi/a)$; and the depletion of the average density of electronic states $N(E)$ for $|E| < \Delta^*$ where $\Delta^*(p)$ diminishes to zero at $p = p*$ (Fig. 1*A*). A mean-field energy gap in the spectrum of coherent $\boldsymbol{k}$-space quasiparticles occurring only near $\boldsymbol{k} \approx (\pm\pi/a, 0); (0, \pm\pi/a, 0)$ could provide a simple phenomenological explanation for virtually all these PG characteristics, but no comprehensive microscopic theory for the PG phase has yet been established.

Extensive evidence has recently emerged for electronic symmetry breaking within the PG phase (Fig. 1*A*). Bulk probes of charge density find translational symmetry breaking in a density wave (DW) state with axial wavevectors $\boldsymbol{Q} = (Q, 0); (0, Q)$ parallel to the CuO_2 axes (1, 2, 5). Similarly, direct visualization with subunit-cell resolution using single-electron tunneling in $Bi_2Sr_2CaCu_2O_8$ and $Ca_{2-x}Na_xCuO_2Cl_2$ reveals intense electronic structure modulations (6, 7) that are locally unidirectional (7, 8), exhibit lattice-commensurate periodicity (9, 10) for all $p < p*$ (11), have a *d*-symmetry form factor (8, 12), and are concentrated at particle-hole symmetric energies (13) $|E| \approx \Delta^*(p)$. The spatial configurations consist of nanoscale regions within which the modulations are commensurate and unidirectional along either (7, 8, 10, 12) $(Q, 0)$ or $(0, Q)$. A complete theoretical explanation for the microscopic origin of these complex atomic-scale electronic structures (6–10, 12) has never been elucidated. Fig. 1*B* shows a representative example of $Z(\boldsymbol{r}, E = \Delta) = N(\boldsymbol{r}, +\Delta)/N(\boldsymbol{r}, -\Delta)$ for this state at $p \approx 8\%$, along with the simultaneously measured topograph $T(\boldsymbol{r})$ at the BiO layer with the Cu sites indicated by crosses. Fig. 1*C*

Significance

By making a variety of quantitative comparisons between electronic visualization experiments and a theory describing coexisting pair density wave and superconductive states in cuprates, we find striking correspondence throughout. Our model can thus explain the microscopic origins of many key atomic-scale phenomena of the cuprate broken-symmetry state. These observations are consistent with the possibility that a short-range pair density wave (PDW) state coexists with superconductivity below a critical hole density in $Bi_2Sr_2CaCu_2O_8$, that the charge density wave modulations in cuprates are a consequence of the PDW state, that the cuprate pseudogap is the antinodal gap of the PDW, and that the critical point in the cuprate phase diagram occurs due to disappearance of the PDW.

Author contributions: P.C., J.C.S.D., and P.J.H. designed research; P.C., S.H.J., K.F., Z.D., S.D.E., M.H.H., H.E., S.U., A.P.M., J.L., J.C.S.D., and P.J.H. performed research; P.C., S.H.J., and P.J.H. analyzed data; and P.C., J.C.S.D., and P.J.H. wrote the paper.

Reviewers: E.B., Weizmann Institute of Science; and H.S., Universidad Autónoma de Madrid.

The authors declare no competing interest.

[1]P.C. and S.H.J. contributed equally to this work.

[2]To whom correspondence may be addressed. Email: jcseamusdavis@gmail.com.

This article contains supporting information online at https://www.pnas.org/lookup/suppl/doi:10.1073/pnas.2002429117/-/DCSupplemental.

First published June 16, 2020.

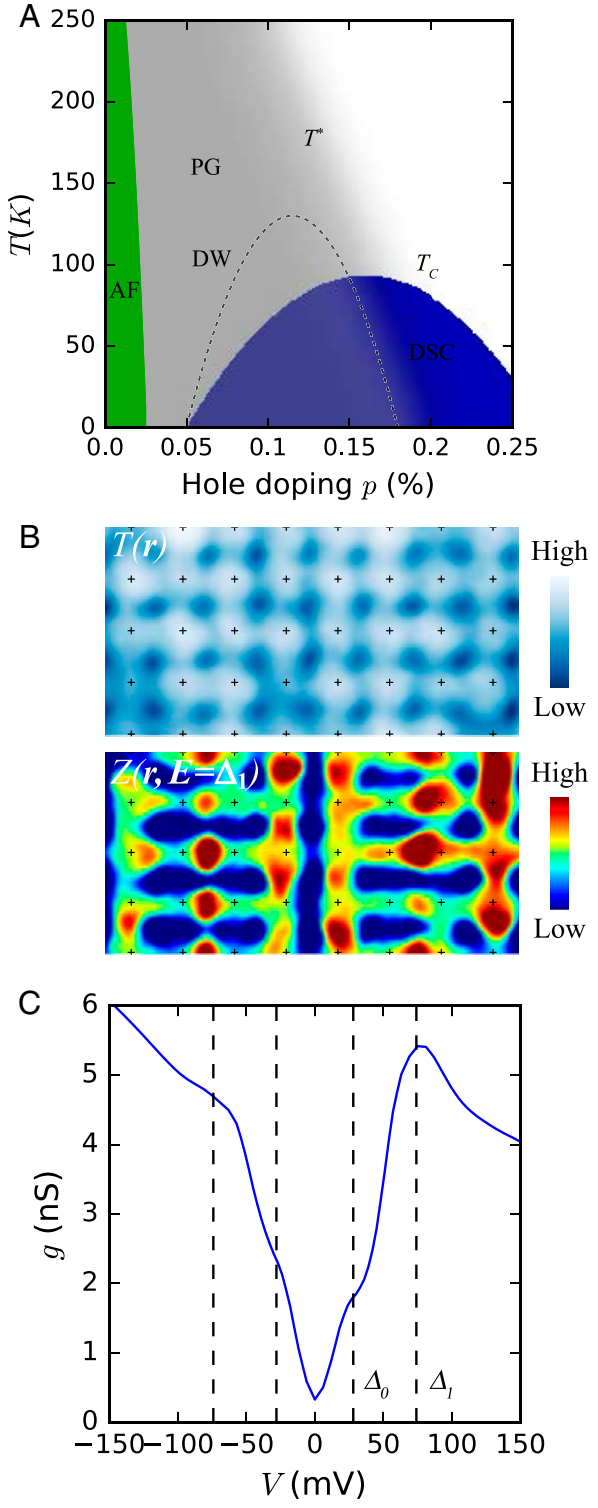

Fig. 1. Broken-symmetry phase coexisting with cuprate superconductivity. (*A*) Schematic phase diagram of lightly hole-doped CuO_2. The Mott insulator phase with long-range AF order disappears quickly with increasing hole doping p to be replaced by the PG phase. The DSC coexists with PG phase below some critical hole density p^*, and persists as a unique state at $p > p^*$. Within the PG phase, the DW modulations have been reported. (*B*) Measured $Z(\mathbf{r},E = \Delta_1)$ at the BiO termination layer of $Bi_2Sr_2CaCu_2O_8$ for $p \sim 0.08$. The locations of Cu atoms of the CuO_2 plane in the same field of view are shown on the topograph $T(r)$ above it. (*C*) Measured differential conductance averaged over the same field of view as *B*. The black dashed lines identify two characteristic energies Δ_1 and Δ_0.

shows the measured differential tunneling conductance $g(E)$ averaged over the whole field of view (FOV) of Fig. 1*B*, and identifies the two characteristic energies Δ_1 and Δ_0. Thus, a key challenge for cuprate studies is to identify microscopically the broken-symmetry state in Fig. 1 *B* and *C* that coexists with the DSC phase and to determine its relationship to the pseudogap.

Because the strong electron–electron interactions subtending the MI state persist even when the long-range AF order disappears (Fig. 1*A*), strong-coupling theory also seems necessary in the PG phase. One frequently recurring consequence (14–22) of such theories is the existence of a state that breaks translational symmetry by modulating the electron-pairing field as

$$\Delta_1(\boldsymbol{r}) = F_P\Delta_1\left[e^{i\boldsymbol{Q}_P\cdot\boldsymbol{r}} + e^{-i\boldsymbol{Q}_P\cdot\boldsymbol{r}}\right]. \quad [1]$$

This is a pair density wave (PDW) state for which Δ_1 is the magnitude of the PDW order parameter and F_P is its form-factor symmetry. Moreover, such a strong-coupling PDW state intertwines (23) the modulations of electron-pair field, of the site/bond charge density, and of spin density. Focus on whether such a PDW state exists in the ground state of cuprates has been further motivated by growing experimental evidence (24–30) that is consistent therewith. Obviously, if this PDW state occurs, it must coexist in the $T \to 0$ ground state together with the robust d-wave superconductivity (Fig. 1*A*). Therefore, an urgent research priority is to understand the atomic-scale electronic structure of a PDW coexisting with a DSC state. This is quite challenging because it requires a theoretical description of PDW + DSC electronic structure at the intraunit-cell scale in $\boldsymbol{r}$-space, and simultaneously throughout a Brillouin zone in $\boldsymbol{k}$-space that is strongly altered by the PDW's existence.

Theory for Cuprate PDW and Coexisting Superconductivity

A classic theory for hole-doped CuO_2 plane electronic structure is based on the t-J model, in which electrons hop with matrix element t between Cu $d_{x^2-y^2}$ orbitals, onsite Coulomb energy $U \to \infty$ to completely prevent their double occupancy, resulting in strong AF exchange interactions $J = 4t^2/U$. Its Hamiltonian is $= -\sum_{(i,j),\sigma} P_G t_{ij}\left(c^\dagger_{i\sigma}c_{j\sigma} + h.c.\right)P_G + J\sum_{<i,j>}\mathbf{S}_i\cdot\mathbf{S}_j$, where the operator P_G projects out all doubly occupied orbitals from the Hilbert space (*SI Appendix*, section A). A renormalized mean-field theory (RMFT) approximation to this t-J model is then of great utility in describing the CuO_2 plane physics (31); it replaces the exact projection P_G operation with renormalization factors g^t_i and g^s_i determined by the average number of charge and spin configurations permissible at every Cu site. The resulting Hamiltonian can be decoupled into a simpler but diagonalizable approximation by using the mean fields describing on-site hole density δ_i, Cu–Cu bond field $\chi_{ij\sigma}$, and electron-pair field $\Delta_{ij\sigma}$(*SI Appendix*, section A). Subsequent variational minimization of the ground-state energy with respect to the unprojected wavefunction $|\Psi_0>$ leads to a set of Bogoliubov–de Gennes (BdG) equations, together with self-consistency conditions on the mean fields. To allow breaking of translational symmetry within RMFT, site-specific and bond-specific renormalization factors $g^t_{i,j}$ and $g^s_{i,j}$ for charge and spin are introduced (17). To obtain a PDW + DSC solution, the BdG equations are initialized with a set of order-parameter fields modulating at wavevector $\boldsymbol{Q}_P = (1/8,0)2\pi/a_0$, and a self-consistent solution is found. From the consequent many-body wavefunction $\Psi_0(\boldsymbol{r})$ of this broken-symmetry state, the net charge on each Cu site

$$\delta_i = 1 - <\Psi_0\left|\sum_\sigma n_{i\sigma}\right|\Psi_0>, \quad [2]$$

the bond field between adjacent Cu sites i,j

$$\chi_{ij\sigma} = \langle \Psi_0 \left| c^{\dagger}_{i\sigma} c_{j\sigma} \right| \Psi_0 \rangle, \quad [3]$$

and the electron-pair field on the bond between adjacent Cu sites i,j

$$\Delta_{ij\sigma} = \sigma \langle \Psi_0 \left| c_{i\sigma} c_{j\bar{\sigma}} \right| \Psi_0 \rangle, \quad [4]$$

can all be calculated. We note that the commensurate PDW + DSC studied here is not the ground state of the cuprate RMFT Hamiltonian, but that its energy above the homogeneous ground state is so tiny (17, 20, 21) (~1 meV per Cu as discussed in *SI Appendix*, section A) that it may be stabilized by a variety of means, including disorder.

Comparison of PDW plus Superconductivity Theory with Experiment

Using this model, we explore the atomic-scale characteristics of a unidirectional, $\lambda = 8a_0$ PDW state coexisting with uniform DSC. Fig. 2*A* shows the predicted hole density δ_i on the Cu sites exhibiting dominant $\lambda = 4a_0$ modulations, together with the projected d-wave superconducting order parameter amplitude Δ_i on the same sites. The corresponding Fourier components of the hole density $\delta(\boldsymbol{q})$ and electron-pair field $\Delta(\boldsymbol{q})$ are shown in Fig. 2*B*. Here it is important to note that the PDW-induced charge modulation amplitude at $\lambda = 8a_0$ is extremely weak for our standard set of parameters (see caption of Fig. 2), whereas the induced charge modulation amplitude at $\lambda = 4a_0$ is dominant. Next, in Fig. 2*C*, we exhibit the projection of the $8a_0$ periodic charge modulations onto the three symmetry-allowed channels *s, s′*, and *d*, utilizing the same definitions as, e.g., in ref. 12 (*SI Appendix*, section A). The charge distribution over the Cu and O sites is clearly characterized by a pronounced d-symmetry form factor (dFF), as has been observed directly in experiments (8, 12).

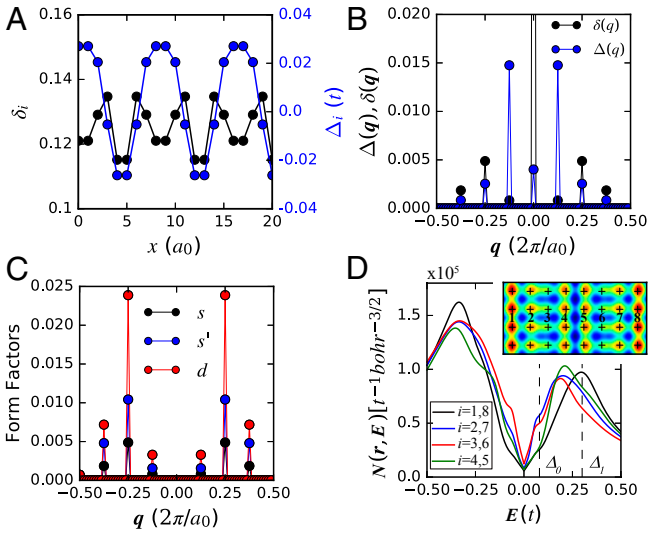

Fig. 2. Characteristic features of our model for a unidirectional PDW + DSC state. (*A*) Variation of hole density (δ) and *d*-wave gap order parameter (Δ) with lattice sites i as obtained from the self-consistent solution of the extended *t-J* model for parameter set doping $x = 0.125$, next-nearest-neighbor (NNN) hopping $t' = -0.3$, exchange interaction $J = 0.3$, and temperature $T = 0.04$. Energy scale is presented in units of nearest-neighbor (NN) hopping t. (*B*) Variation of hole density (δ) and *d*-wave gap-order parameter (Δ) with wavevector $\boldsymbol{q}$ obtained by Fourier transforming corresponding lattice-space quantities shown in *A*. Hole density and gap-order parameter show largest modulating components at $|\boldsymbol{q}| = 0.25$ and $|\boldsymbol{q}| = 0.125$, respectively. But, the predicted $|\boldsymbol{q}| = 0.125$ component of charge density modulation $\delta(\boldsymbol{q})$ is extremely small, due to the small uniform component of the gap-order parameter. Wavevectors are presented in units of $2\pi/a_0$, where a_0 is the lattice constant in the CuO_2 *a-b* plane. (*C*) dFFs obtained from the hole-density and NN bond-order parameter (χ). The dFF is dominant at all wavevectors, with predominant intensity at $|\boldsymbol{q}| = 0.25$. (*D*) Continuum local density of states $N(r,E)$ at Cu positions along Cu-O_x direction over a period of PDW ($8a_0$). Here $\Delta_1 \sim 0.3$ and $\Delta_0 \sim 0.07$ correspond to the gap scale associated with the PDW component and uniform DSC component of the PDW + DSC state, respectively. *Inset* shows $N(\boldsymbol{r}, E = \Delta_1)$ map, where Cu positions are marked with crosses.

For comparison with underdoped $Bi_2Sr_2CaCu_2O_8$ measurements, we next use the RMFT PDW + DSC model and evaluate its quasiparticle states with intraunit-cell resolution using a Wannier function-based method (21, 22). This is designed to allow quantitative predictions of electronic structure in $\boldsymbol{r}$-space, $\boldsymbol{q}$-space, and $\boldsymbol{k}$-space of a PDW + DSC state. The band structure parametrization is $t = 400$ meV, $t' = -0.3t$, and $J = 0.3t$, all representing $Bi_2Sr_2CaCu_2O_8$ at $p \approx 0.08$. For this parameter set, we calculate the quasiparticle Green's functions in the self-consistently obtained PDW + DSC state, with the unidirectional PDW wavevector $\boldsymbol{Q_P} = (1/8,0)2\pi/a_0$ that is modulating parallel to the x axis but lattice-periodic along the y axis, and find the PDW spectral gap $\Delta_1 \approx 0.3t \approx 100$ meV, and gap associated with uniform DSC $\Delta_0 \approx 0.07t \approx 25$ meV (*SI Appendix*, section A). Moreover, while almost all previous RMFT studies of cuprates yield only the Cu site-specific Green's function matrix $G_{ij\sigma}(E)$ within the CuO_2 plane, the experimental measurements of electron-tunneling probability are actually made at a continuum of locations just above the crystal termination BiO layer of $Bi_2Sr_2CaCu_2O_8$ (Fig. 1*B*). Therefore, we use first-principles Cu $d_{x^2-y^2}$ Wannier functions $W_i(\boldsymbol{r})$ to make quantitative predictions of the $\boldsymbol{r}$-space Green's functions $G_\sigma(\boldsymbol{r},E) = \sum_{ij} G_{ij\sigma}(E) W_i(\boldsymbol{r}) W_j^*(\boldsymbol{r})$ of a PDW + DSC state, everywhere at a height 0.4 nm above BiO terminal plane (32, 33) (*SI Appendix*, section B). We emphasize that none of the mean fields δ_i, $\chi_{ij\sigma}$, and $\Delta_{ij\sigma}$ are related simply to the local quasiparticle density of states $N(\boldsymbol{r},E) = \sum_\sigma -\frac{1}{\pi} \mathrm{Im}\, G_\sigma(\boldsymbol{r},E)$, which must instead be determined from the Bogoliubov quasiparticle eigenstates (20, 21, 24, 25, 28, 34–36) that enter the lattice Green's function $G_{ij\sigma}$. Fig. 2*D* shows the theoretical $N(\mathbf{r},E)$ for the PDW + DSC state at various points in the modulated state, as identified in the inset. Note that a shoulderlike feature is present at nearly identical particle-hole symmetric energies $\pm\Delta_0$ for all Cu sites, such that we associate it with the uniform d-wave superconducting condensate DSC. By contrast, this model predicts that the energy Δ_p at which the "coherence peak" occurs $(E > 0)$ varies from atom to atom in real space; its largest magnitude may be associated with the PDW amplitude Δ_1.

The bias dependence of $Z(\boldsymbol{r},E) = N(\boldsymbol{r},+E)/N(\boldsymbol{r},-E)$ from our PDW + DSC model are then predicted for comparison with experiment. Fig. 3 *A–F* show these $Z(\boldsymbol{r},E)$ data focusing on the energy range $0.5\Delta_1 \lesssim E \lesssim 1.5\Delta_1$, within which they exhibit a comprehensive dFF (*SI Appendix*, section B). This effect can be seen directly because the model $Z(\boldsymbol{r},E)$ has intraunit-cell precision. Consider the three sublattices making up the primary features of the $Z(\boldsymbol{r},E)$ image: $Cu(\boldsymbol{r},E)$ containing only $Z(\boldsymbol{r},E)$ at copper sites and $O_x(\boldsymbol{r},E)$ and $O_y(\boldsymbol{r},E)$, containing only $Z(\boldsymbol{r},E)$ at the *x*/*y* axis oxygen sites. By definition, in a dFF charge density wave, modulations on the $O_x(\boldsymbol{r},E)$ and $O_y(\boldsymbol{r},E)$ sites are out of phase by π. In our PDW + DSC model, such phenomena occur at $2\boldsymbol{Q_P}$, first appear near $E \approx \Delta_1/2$, are intense surrounding $E \approx \Delta_1$, and eventually disappear near $E \approx 2\Delta_1$ (*SI Appendix*, section B and ref. 8). This energy dependence, including both the dominance of the dFF in a wide range of energies surrounding Δ_1, as well as the low-energy dominance of the s' form factor, were demonstrated earlier using the same theory (21) but for an incommensurate wavevector.

For experimental comparison with our PDW + DSC model, we visualize the electronic structure (37) using spectroscopic

PHYSICS

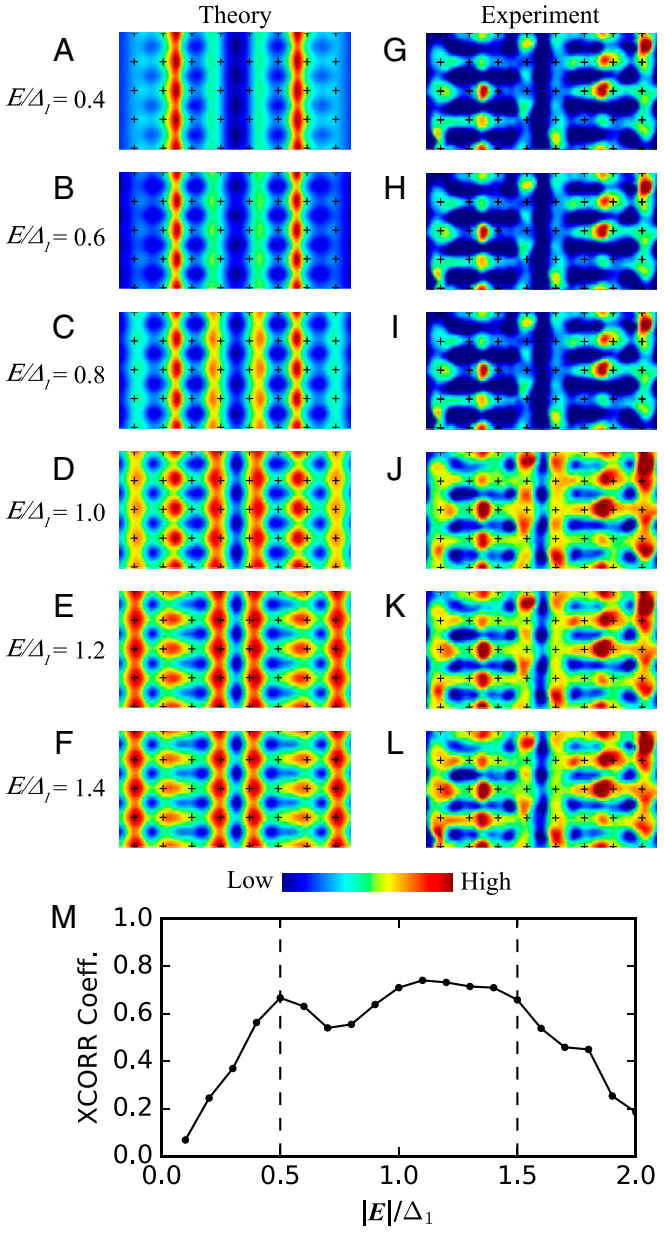

Fig. 3. $Z(r,E)$ in PDW + DSC state compared to corresponding experimental data. (*A–F*) Predicted $Z(r,E)$ maps in PDW + DSC state for the terminal BiO layer, at energies $|E| = 0.4\Delta_1$, $0.6\Delta_1$, $0.8\Delta_1$, Δ_1, $1.2\Delta_1$, and $1.4\Delta_1$, respectively. (*G–L*) Experimentally measured $Z(r,E)$ maps at the terminal BiO layer, for bias voltages corresponding to energies in *A–F*, respectively. (*M*) Cross-correlation coefficient between theoretical $Z(r,E)$ images and experimental $Z(r,E)$ map images as a function of energy/voltage, showing very strong correspondence between them in the region ($0.5\Delta_1$ $-1.5\Delta_1$, marked with vertical black dashed lines) around PDW energy gap scale. Direct examination of a typical pair, for example (*E*) and (*K*), show why the cross-correlation coefficient is so high. A wide variety of minute details, including the distinct broken-rotational symmetry inside each specific CuO_2 unit cell, the *d*-symmetry modulations of this broken symmetry over eight unit cells, and the bond-centered register of this $8a_0$ unit to the CuO_2 lattice, correspond strikingly between experiment and theory.

imaging STM (SISTM) measurements of STM–tip-sample differential electron tunneling conductance $dI/dV(\boldsymbol{r},V) \equiv g(\boldsymbol{r},V)$. We study the terminal BiO layer of $Bi_2Sr_2CaCu_2O_8$ for a range of tip-sample voltage differences V and at $T = 4.2$ K. In theory, $g(\boldsymbol{r},V) \propto N(\boldsymbol{r},E)/\int_0^{eV_s} N(\boldsymbol{r},E)dE$ (V_s is the junction-formation voltage). The ratio $Z(\boldsymbol{r},V) = g(\boldsymbol{r},+V)/g(\boldsymbol{r},-V)$ is widely used in such visualization studies because, even if $\int_0^{eV_s} N(\boldsymbol{r},E)dE$ is heterogeneous, it yields a valid measure of periodicities and broken symmetries (37). Fig. 3 *G–L* show the measured $Z(\boldsymbol{r},E)$ in the energy range $0.5\Delta_1 \lesssim E \lesssim 1.5\Delta_1$, with each panel shown side-by-side with the equivalent energy in the model. The most intense modulations occur at $E \approx \Delta_1(p)$ for all $p < 0.19$ (8, 13), and all through this energy range they exhibit a comprehensive dFF (8, 12, 13). Therefore, correspondence between theoretical $Z(\boldsymbol{r},E)$ from the PDW + DSC model (Fig. 3 *A–F*) and the measured $Z(\boldsymbol{r},E)$ (Fig. 3 *G–L*) is observed to be excellent over a wide energy range. This can be quantified by measuring the cross-correlation value of each pair of theory: experiment $Z(\boldsymbol{r},E/\Delta_1)$ images. The result, shown in Fig. 3*M*, demonstrates strong cross-correlations between theory–experiment pairs of $Z(\boldsymbol{r},E)$ images throughout the energy range. Therefore, predictions of PDW + DSC theory, on distance scales ranging from $8a_0$ down to subunit cell, correspond strongly and in detail to the complex patterns of quasiparticle states observed in the broken-symmetry state of $p < p^*$ $Bi_2Sr_2CaCu_2O_8$.

Next, as seen in Fig. 2*D*, the theory predicts that coherence peak energy Δ_p varies substantially from one unit cell to the next within the $\lambda = 8a_0$ PDW. In Fig. 4*A* we show the theoretical gap map for the PDW + DSC state obtained by identifying the coherence peak energy $\Delta_p(r)$ for $E > 0$ at all intraunit-cell points over an area of 8×12 unit cells, while Fig. 4*B* shows the gap map obtained by using the same algorithm to determine $\Delta_p(r)$ from measured dI/dV spectra. Both theory and experiment show $8a_0$ periodic $\Delta_p(r)$ modulations within which there are smaller atomically resolved variations that exhibit common characteristics but are not identical, most likely because of inadequacies in the density functional theory-derived Wannier functions in representing underdoped cuprates.

Finally, we consider the effects of a PDW + DSC state on Bogoliubov quasiparticle scattering interference (38) (BQPI). This occurs when an impurity atom scatters quasiparticles, which then interfere to produce characteristic modulations of $N(\boldsymbol{r},E)$ surrounding each impurity atom. Local maxima in $Z(\boldsymbol{q},E)$, the power-spectral-density Fourier transform of $Z(\boldsymbol{r},E)$, reveal the sets of energy-dispersive wavevectors $\boldsymbol{q}_i(E)$ generated by the scattering interference (11). A BQPI data set thus consists of a sequence of $Z(\boldsymbol{q},E)$ images spanning the energy range of interest, from which an efficient synopsis over all of the QPI modulations can be achieved (11) using $\Lambda(\boldsymbol{q},\Delta) = \sum_{E=0}^{\Delta} Z(\boldsymbol{q},E)$. The key utility here is that $\Lambda(\boldsymbol{q},\Delta)$ provides an efficient and characteristic "fingerprint" of whatever ordered state(s) controls the $\boldsymbol{q}_i(E)$ of the BQPI processes. For our PDW + DSC model, we calculate $Z(\boldsymbol{q},E)$ using a simple pointlike scatterer within the RMFT framework (*SI Appendix*, section C). From these model $Z(\boldsymbol{q},E)$ images, the predicted $\Lambda(\boldsymbol{q},\Delta_0) = \sum_{E=0}^{\Delta_0} Z(\boldsymbol{q},E)$ is determined and shown in Fig. 5*A*. This contains the overall $\Lambda(\boldsymbol{q},\Delta_0)$ fingerprint expected of the BQPI in this PDW + DSC state. For comparison, Fig. 5*B* includes the predicted $\Lambda(\boldsymbol{q},\Delta_0)$ of a simple *d*-wave superconductor with a Fermi surface at $p = 23\%$. It reflects the familiar peaks characteristic of dispersing Bogoliubov quasiparticles, including the tracing of the Fermi surface by the peak conventionally labeled $\boldsymbol{q}_4$ as bias voltage is varied (11). Clearly, the PDW + DSC $\Lambda(\boldsymbol{q},\Delta_0)$ in Fig. 5*A* is very different, exhibiting very weak dispersion and thus producing sharper $\boldsymbol{q}$-space spots, as well as the absence of any $\boldsymbol{q}_4$ scattering interference near edges of $\boldsymbol{q}$-space reciprocal unit cell. To compare these predictions for $\Lambda(\boldsymbol{q},\Delta_0)$ with and without the PDW order to experiments, we show measured $\Lambda(\boldsymbol{q},\Delta_0) = \sum_{E\cong 0}^{\Delta_0} Z(\boldsymbol{q},E)$ for both low p

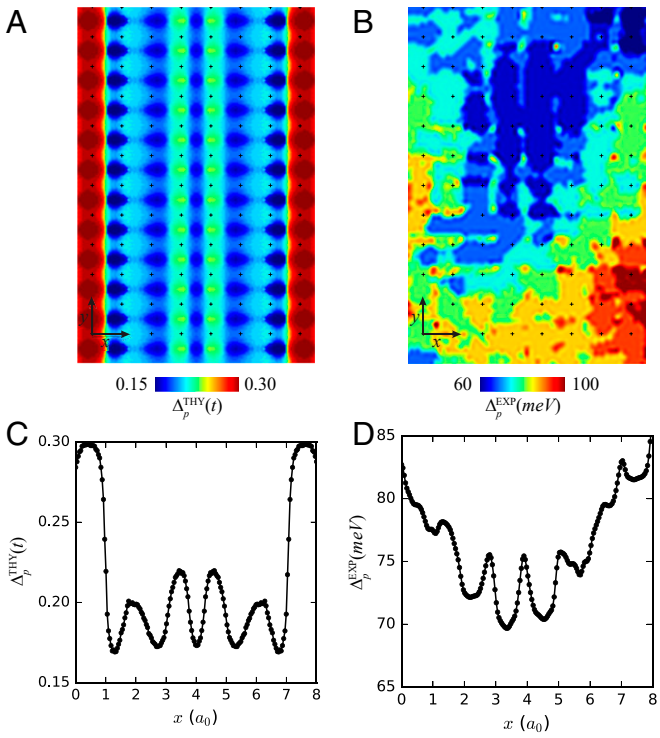

Fig. 4. Gap map $\Delta_p(\boldsymbol{r})$ derived from coherence-peak energy in PDW + DSC state. (*A*) Gap map in PDW + DSC state obtained by identifying coherence peak energy $\Delta_p(\boldsymbol{r})$ for $E > 0$ at all intraunit-cell points over an area of 8×12 unit cells. Color bar is given in the units of *t*. (*B*) Gap map $\Delta_p(\boldsymbol{r})$ obtained by following the same procedure as in *A*, but for experimentally measured $g(\boldsymbol{r},V)$ spectra of a representative domain as shown. (*C*) Gap $\Delta_p(\boldsymbol{r})$ averaged along *y* direction obtained in the PDW + DSC model. (*D*) Gap $\Delta_p(\boldsymbol{r})$ averaged along *y* direction obtained from the $g(\boldsymbol{r},V)$ spectra.

and high *p* in Fig. 5 *C* and *D*. The very distinct characteristics of $\Lambda(\boldsymbol{q},\Delta_0)$ observed at low *p* and high *p*, are in striking agreement with the PDW + DSC model predictions for $\Lambda(\boldsymbol{q},\Delta_0)$ with and without the PDW state, respectively. Moreover, the empirical BQPI phenomena in Fig. 5*C* are a characteristic of the pseudogap region of the phase diagram (11), whereas the PDW + DSC model that predicts them (Fig. 5*A*) does not require a separate pseudogap to be introduced because the $\boldsymbol{k}$-space structure of the PDW is what gaps antinodes (34). Finally, in our PDW + DSC model, we find that increasing *p* leads to an instability of the PDW order toward a uniform DSC state via a weak first-order transition at $p \approx 0.18$ (*SI Appendix*, section A), whereas the experimentally observed disappearance of translational symmetry breaking simultaneous with the reappearance of low-energy quasiparticles at the antinodes (11), occurs at $p \approx 0.19$.

PDW plus Superconductivity Theory and Other Techniques

We note that NMR and X-ray studies (primarily of $YBa_2Cu_3O_7$ and La_2BaCuO_4) (39) appear consistent with SISTM visualizations of incommensurate electronic density modulations (primarily of $Bi_2Sr_2CaCu_2O_8$ and $Ca_{2-x}Na_xCuO_2Cl_2$) (37), and to have a common microscopic cause (40, 41). But in our current study, we have compared carefully to atomic scale studies of $Bi_2Sr_2CaCu_2O_8$ that manifest short-range commensurate periodicity in electronic structure images (7, 9, 10, 12). These two phenomenologies may appear mutually contradictory. However, the X-ray and Fourier transform STM (FTSTM) studies focus only on a specific wavevector, and this procedure discards all of the other information distributed throughout $\boldsymbol{q}$-space. In $Bi_2Sr_2CaCu_2O_8$, those data actually contain the extremely complex information on the effects of form factor symmetry, and on how the commensurate, unidirectional electronic-structure patterns proliferate throughout real space (10). Thus, the coexistence of a local maximum at incommensurate wavevector in X-ray or FTSTM measurements, with commensurate electronic structures distributed throughout real space, is a demonstrable characteristic of $Bi_2Sr_2CaCu_2O_8$ electronic structure (10). The most likely resolution is that the measured incommensurate behavior in X-ray or FTSTM experiments represent quite discommensurate behavior, where commensurate, unidirectional DWs are coupled by random phase slips. Indeed, by using advanced techniques, these phase slips are identifiable directly in the $N(\boldsymbol{r},E)$ modulations of $Bi_2Sr_2CaCu_2O_8$ (9). Another interesting and related issue is the existence or nonexistence of an X-ray scattering peak at $\boldsymbol{Q} = 2\pi/a_0(1/8,0)$, because this is one of the indications that charge density wave (CDW) modulations are induced by $\lambda = 8a_0$ PDW order in the presence of DSC. Although such a peak has been observed for $N(\boldsymbol{r},E)$ both within vortex halos (30) and at zero field (42) in $Bi_2Sr_2CaCu_2O_8$, attempts to detect it by X-ray measurements on $YBa_2Cu_3O_7$ at zero field have not yet succeeded. Importantly, one of the revelations of our PDW + DSC model is that only a tiny $\boldsymbol{Q} = 2\pi/a_0(1/8,0)$ charge modulation peak is predicted (black in Fig. 2*B*), whose intensity may be below present X-ray detection limits. Alternatively, the PDW in $YBa_2Cu_3O_7$ may be fluctuating and thus unobservable (43). A distinct point is that a uniform DSC + PDW state should have clear spectroscopic signatures visible in angle-resolved photoemission spectroscopy (ARPES) (24, 28). And, to first order, the PDW + DSC model and ARPES correspond well, because the strong antinodal gap due to the PDW is empirically indistinguishable from the antinodal "pseudogap" reported by virtually all ARPES studies. But, some fine features the PDW + DSC model predicts for $A(\boldsymbol{k},\omega)$ have not yet been seen by ARPES, presumably due to the short-range nature

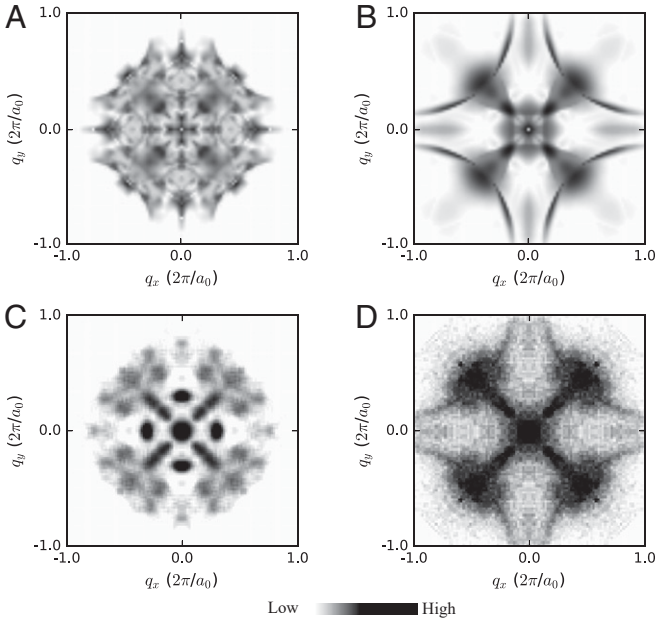

Fig. 5. Comparison of $\Lambda(\boldsymbol{q},\Delta_0)$ predictions/data in PDW + DSC and pure DSC states. (*A*) Predicted $\Lambda(\boldsymbol{q},\Delta_0)$ map in PDW + DSC state at doping $x = 0.125$. (*B*) Predicted $\Lambda(\boldsymbol{q},\Delta_0)$ map in a uniform *d*-wave superconductor state at doping $x = 0.23$. (*C*) Experimental $\Lambda(\boldsymbol{q},\Delta_0)$ map for underdoped $Bi_2Sr_2CaCu_2O_8$ at $p = 0.08 \pm 0.01$. In principle $T(\boldsymbol{q}, \text{eV} = \Delta_0)$, the Fourier transform of a topographic image $T(\boldsymbol{r}, \text{eV} = \Delta_0)$, would be logarithmically sensitive to the same information as $\Lambda(\boldsymbol{q},\Delta_0)$. But, because it also contains such intense signals from a variety of other phenomena, is has proven difficult to use that approach for QPI studies. (*D*) Experimental $\Lambda(\boldsymbol{q},\Delta_0)$ map for overdoped $Bi_2Sr_2CaCu_2O_8$ at $p = 0.23$.

of the static PDW + DSC patches. Future theoretical modeling studies of disordered PDWs will be necessary to explore these issues. Lastly, one may wonder whether a $4a_0$ periodic CDW state coexisting with a d-wave superconductor could reproduce the $N(\boldsymbol{r},E)$ and $Z(\boldsymbol{r},E)$ data or the $\Lambda(\boldsymbol{q},\Delta_0)$ QPI signatures, as well as our PDW + DSC model. In that regard, we find that one must initialize the RMFT equations with a modulating pair field to converge to a nonuniform state and that any other type of initialization, for example a $4a_0$ periodic CDW, converges only to a uniform DSC. More generally, Ginzburg–Landau models based on a large DSC order parameter coexisting with a CDW of wavevector $\boldsymbol{Q}_{CDW}$ (and possibly an induced PDW at $\boldsymbol{Q}_{CDW}$), do not have PDW at $\boldsymbol{Q}_{CDW}/2$. Moreover, when we use our RMFT approach to study such CDW + DSC driven states, we find in two cases that the predicted $Z(\boldsymbol{r},E)$ spectra show very poor correlation with equivalent experiments (*SI Appendix*, section D). Therefore, the observation of $8a_0$ periodic modulations in $Z(\boldsymbol{r},E)$ and $\Delta_p(\boldsymbol{r})$ along with a particle-hole symmetric kink at low energies, all of which are characteristics of the RMFT-based PDW + DSC model but not of the others, favor the interpretation based on a PDW coexisting with superconductivity.

Discussion and Conclusions

To recapitulate, we have developed a strong-coupling mean-field theory for a coexisting d-wave superconductor and PDW ($\lambda = 8a_0$) and made detailed comparisons of its predictions with experimental SISTM data from $Bi_2Sr_2CaCu_2O_8$. To allow valid quantitative comparison to such experiments, the atomic-scale tunneling characteristics of the PDW + DSC state at the BiO termination layer of the crystal were predicted utilizing a recently developed Wannier-function-based method. Then, from the $8a_0$ scale down to inside the CuO_2 unit cell, we find that the predictions (Figs. 2 *A–D* and 3 *A–F*) correspond strikingly well with the highly complex electronic structure patterns observed by SISTM (Fig. 3 *G–L*) in the $p < p^*$ broken-symmetry state of $Bi_2Sr_2CaCu_2O_8$. Indeed, the PDW + DSC model explains simply the microscopic origins of many enigmatic characteristics of this broken-symmetry state, including the $\lambda = 4a_0$ dFF $N(\boldsymbol{r},E)$ modulations (6–10, 12), the concentration of their amplitude maxima (8, 9, 12, 13) surrounding $|E| = \Delta_1$, and the $8a_0$ periodic energy gap modulations observed in the superconducting state (42). Further, by considering scattering of $\boldsymbol{k}$-space quasiparticles, we explore the QPI fingerprint $\Lambda(\boldsymbol{q},\Delta_0)$ of the PDW + DSC model (Fig. 5*A*), and find it too in strong, detailed agreement with measured $\Lambda(\boldsymbol{q},\Delta_0)$ (Fig. 5*C*). Hence, the antinodal pseudogap that dominates the experimental data $\Lambda(\boldsymbol{q},\Delta_0)$ (Fig. 5*C*) plausibly corresponds to the antinodal gap of the PDW in the model $\Lambda(\boldsymbol{q},\Delta_0)$ (Fig. 5*A*). Further, the transition at $p \approx 18\%$ in the model from the $\Lambda(\boldsymbol{q},\Delta_0)$ characteristic of a PDW + DSC state (Fig. 5*A*) to that of a pure d-wave superconductor (Fig. 5*B*) corresponds qualitatively with the experimentally observed (11) transition in $\Lambda(\boldsymbol{q},\Delta_0)$ at $p \approx p*$ (Fig. 5 *C* and *D*). Consequently, the disappearance at a critical hole density p^* of both the $\boldsymbol{r}$-space symmetry-breaking structures (Fig. 3 *A–F*) and the concomitant $\boldsymbol{q}$-space QPI signatures (Fig. 5*C*) are all features that occur in the PDW + DSC model at the hole density where the PDW disappears. Overall, the agreement between our PDW + DSC model and the plethora of experimental characteristics is consistent with a picture in which a disordered $\lambda = 8a_0$ PDW + DSC state exists for $p < p*$ in $Bi_2Sr_2CaCu_2O_8$, the $\lambda = 4a_0$ charge modulations observed by X-ray scattering (5, 39) are a consequence of this state, the cuprate pseudogap coincides with the antinodal gap of the coexisting PDW, and the cuprate $p \approx p^*$ critical point is due to disappearance of the PDW.

Data Availability. All data used in this study are available upon request from the corresponding author.

ACKNOWLEDGMENTS. The authors acknowledge and thank D. Agterberg, E.-A. Kim, M. Norman, S.A. Kivelson, and Y. Wang for very helpful discussions and advice. P.C. and P.J.H. acknowledge support from research grant NSF-DMR-1849751. P.C. acknowledges the research grant PDF/2017/002242 from Science and Engineering Research Board, Department of Science and Technology (SERB, DST), India. S.U. and H.E. acknowledge support from a Grant-in-aid for Scientific Research from the Ministry of Science and Education (Japan) and the Global Centers of Excellence Program for Japan Society for the Promotion of Science. S.H.J. and J.L. acknowledge support from the Institute for Basic Science in Korea (Grant IBS-R009-G2), the Institute of Applied Physics of Seoul National University, National Research Foundation of Korea grant funded by the Korea government Ministry of Science, ICT and Future Planning (MSIP) (2017R1A2B3009576). S.H.J. also acknowledges support from the BK21 Plus Project. K.F. and Z.D. acknowledge support from the US Department of Energy, Office of Basic Energy Sciences, under Contract DEAC02-98CH10886; J.C.S.D. acknowledges support from the Moore Foundation's Emergent Phenomena in Quantum Systems (EPiQS) Initiative through Grant GBMF9457, from Science Foundation Ireland under Award SFI 17/RP/5445, and from the European Research Council under Award DLV-788932.

1. B. Keimer, S. A. Kivelson, M. R. Norman, S. Uchida, J. Zaanen, From quantum matter to high-temperature superconductivity in copper oxides. *Nature* **518**, 179–186 (2015).
2. R. Comin, A. Damascelli, Resonant X-ray scattering studies of charge order in cuprates. *Annu. Rev. Condens. Matter Phys.* **7**, 369–405 (2016).
3. M. R. Norman, D. Pines, C. Kallin, The pseudogap: Friend or foe of high T_c? *Adv. Phys.* **54**, 715–733 (2005).
4. P. A. Lee, N. Nagaosa, X.-G. Wen, Doping a Mott insulator: Physics of high-temperature superconductivity. *Rev. Mod. Phys.* **78**, 17 (2006).
5. A. Frano, S. Blanco-Canosa, B. Keimer, R. Birgeneau, Charge ordering in superconducting copper oxides. *J. Phys. Condens. Matter*, 10.1088/1361-648X/ab6140 (2019).
6. T. Hanaguri *et al.*, A "checkerboard" electronic crystal state in lightly hole-doped $Ca_{2-x}Na_xCuO_2Cl_2$. *Nature* **430**, 1001–1005 (2004).
7. Y. Kohsaka *et al.*, An intrinsic bond-centered electronic glass with unidirectional domains in underdoped cuprates. *Science* **315**, 1380–1385 (2007).
8. M. H. Hamidian *et al.*, Atomic-scale electronic structure of the cuprate d-symmetry form factor density wave state. *Nat. Phys.* **12**, 150–156 (2015).
9. A. Mesaros *et al.*, Commensurate $4a_0$-period charge density modulations throughout the $Bi_2Sr_2CaCu_2O_{8+x}$ pseudogap regime. *Proc. Natl. Acad. Sci. U.S.A.* **113**, 12661–12666 (2016).
10. Y. Zhang *et al.*, Machine learning in electronic-quantum-matter imaging experiments. *Nature* **570**, 484–490 (2019).
11. K. Fujita *et al.*, Simultaneous transitions in cuprate momentum-space topology and electronic symmetry breaking. *Science* **344**, 612–616 (2014).
12. K. Fujita *et al.*, Direct phase-sensitive identification of a d-form factor density wave in underdoped cuprates. *Proc. Natl. Acad. Sci. U.S.A.* **111**, E3026–E3032 (2014).
13. S. Mukhopadhyay *et al.*, Evidence for a vestigial nematic state in the cuprate pseudogap phase. *Proc. Natl. Acad. Sci. U.S.A.* **116**, 13249–13254 (2019).
14. A. Himeda, T. Kato, M. Ogata, Stripe states with spatially oscillating *d*-wave superconductivity in the two-dimensional *t-t'-J* model. *Phys. Rev. Lett.* **88**, 117001 (2002).
15. M. Raczkowski, M. Capello, D. Poilblanc, R. Frésard, A. M. Oleś, Unidirectional *d*-wave superconducting domains in the two-dimensional *t-J* model. *Phys. Rev. B* **76**, 140505 (2007).
16. E. Berg *et al.*, Dynamical layer decoupling in a stripe-ordered high-T_c superconductor. *Phys. Rev. Lett.* **99**, 127003 (2007).
17. K.-Y. Yang, W. Q. Chen, T. M. Rice, M. Sigrist, F.-C. Zhang, Nature of stripes in the generalized *t–J* model applied to the cuprate superconductors. *New J. Phys.* **11**, 55053 (2009).
18. F. Loder, S. Graser, A. P. Kampf, T. Kopp, Mean-field pairing theory for the charge-stripe phase of high-temperature cuprate superconductors. *Phys. Rev. Lett.* **107**, 187001 (2011).
19. P. Corboz, T. M. Rice, M. Troyer, Competing states in the *t-J* model: Uniform D-wave state versus stripe state. *Phys. Rev. Lett.* **113**, 46402 (2014).
20. W.-L. Tu, T.-K. Lee, Genesis of charge orders in high temperature superconductors. *Sci. Rep.* **6**, 18675 (2016).
21. P. Choubey, W.-L. Tu, T.-K. Lee, P. J. Hirschfeld, Incommensurate charge ordered states in the *t–t'–J* model. *New J. Phys.* **19**, 13028 (2017).
22. S. Verret, M. Charlebois, D. Sénéchal, A.-M. S. Tremblay, Subgap structures and pseudogap in cuprate superconductors: Role of density waves. *Phys. Rev. B* **95**, 54518 (2017).
23. E. Fradkin, S. A. Kivelson, J. M. Tranquada, Colloquium: Theory of intertwined orders in high temperature superconductors. *Rev. Mod. Phys.* **87**, 457 (2015).
24. P. A. Lee, Amperean pairing and the pseudogap phase of cuprate Superconductors. *Phys. Rev. X* **4**, 31017 (2014).
25. Q. Li, M. Hücker, G. D. Gu, A. M. Tsvelik, J. M. Tranquada, Two-dimensional superconducting fluctuations in stripe-ordered $La_{1.875}Ba_{0.125}CuO_4$. *Phys. Rev. Lett.* **99**, 67001 (2007).
26. E. Berg, E. Fradkin, S. A. Kivelson, Charge-4e superconductivity from pair-density-wave order in certain high-temperature superconductors. *Nat. Phys.* **5**, 830–833 (2009).

27. E. Berg, E. Fradkin, S. A. Kivelson, J. M. Tranquada, Striped superconductors: How spin, charge and superconducting orders intertwine in the cuprates. *New J. Phys.* **11**, 115004 (2009).
28. M. R. Norman, J. C. S. Davis, Quantum oscillations in a biaxial pair density wave state. *Proc. Natl. Acad. Sci. U.S.A.* **115**, 5389–5391 (2018).
29. M. H. Hamidian *et al*., Detection of a Cooper-pair density wave in $Bi_2Sr_2CaCu_2O_{8+x}$. *Nature* **532**, 343–347 (2016).
30. S. D. Edkins *et al*., Magnetic field-induced pair density wave state in the cuprate vortex halo. *Science* **364**, 976–980 (2019).
31. F. C. Zhang, C. Gross, T. M. Rice, H. Shiba, A renormalised Hamiltonian approach to a resonant valence bond wavefunction. *Supercond. Sci. Technol.* **1**, 36 (1988).
32. P. Choubey, T. Berlijn, A. Kreisel, C. Cao, P. J. Hirschfeld, Visualization of atomic scale phenomena in superconductors: Application to FeSe. *Phys. Rev. B* **90**, 134520 (2014).
33. P. Choubey, A. Kreisel, T. Berlijn, B. M. Andersen, P. J. Hirschfeld, Universality of scanning tunneling microscopy in cuprate superconductors. *Phys. Rev. B* **96**, 174523 (2017).
34. S. Baruch, D. Orgad, Spectral signatures of modulated *d*-wave superconducting phases. *Phys. Rev. B* **77**, 174502 (2008).
35. Y. Wang, D. F. Agterberg, A. Chubukov, Coexistence of charge-density-wave and pair-density-wave orders in underdoped cuprates. *Phys. Rev. Lett.* **114**, 197001 (2015).
36. W.-L. Tu, T.-K. Lee, Evolution of pairing orders between pseudogap and superconducting phases of cuprate superconductors. *Sci. Rep.* **9**, 1719 (2019).
37. K. Fujita *et al*., "Spectroscopic imaging STM: Atomic-scale visualization of electronic structure and symmetry in underdoped cuprates" in *Strongly Correlated Systems–Experimental Techniques*, A. Avella, F. Mancini, Eds. (Springer, Berlin, 2015), Vol. 180, pp. 73–109.
38. Q.-H. Wang, D.-H. Lee, Quasiparticle scattering interference in high-temperature superconductors. *Phys. Rev. B* **67**, 20511 (2003).
39. H. Miao *et al*., Formation of incommensurate charge density waves in cuprates. *Phys. Rev. X* **9**, 31042 (2019).
40. R. Comin *et al*., Charge order driven by Fermi-arc instability in $Bi_2Sr_{(2-x)}La_{(x)}CuO_{(6+\delta)}$. *Science* **343**, 390–392 (2014).
41. E. H. da Silva Neto *et al*., Ubiquitous interplay between charge ordering and high-temperature superconductivity in cuprates. *Science* **343**, 393–396 (2014).
42. Z. Du *et al*., Imaging the energy gap modulations of the cuprate pair-density-wave state. *Nature* **580**, 65–70 (2020).
43. Z. Dai, T. Senthil, P. A. Lee, Modeling the pseudogap metallic state in cuprates: Quantum disordered pair density wave. *Phys. Rev. B* **101**, 064502 (2020).